JOURNAL OF MATERIALS SCIENCE 33 (1998) 1003–1013

Synthesis and properties analysis of char-reinforced Al–13.5Si–2.5Mg alloy composites

J. U. EJIOFOR, R. G. REDDY
Department of Metallurgical and Materials Engineering, The University of Alabama, PO Box 870202, Tuscaloosa, AL 35487 USA

B. A. OKORIE
Department of Materials and Metallurgical Engineering, Enugu State University of Technology, PMB 01660, Nigeria

The re-evaluation of previous and existing methods in materials processing is becoming ever more critical because of processing and starting materials cost factors. A study on the synthesis and properties investigation of hypereutectic Al–13.5Si–2.5Mg alloy reinforced with carbon chars using coconut shell as the organic precursor has been carried out. The low-cost, double compaction solid-state technique was used. Reinforcing the hypereutectic alloy with coconut shell char particles (size: < 140 μm) at 2 vol % and consolidating by reaction sintering at 600 °C in vacuum for 15 min, followed by near net-shape compaction at 250 MPa, increased the hardness of the alloy 6% while reducing its strength (UTS) by only 3%. The use of palm kernel shell char as the dispersed phase was found to yield identical results. At 2 vol % char, the mechanical properties, sintered density and dimensional changes were optimally found to be suitable for lightweight anti-friction electromechanical applications. Attempts to reinforce the alloy with 2 vol % coconut shell chars activated in CO_2 reduced its strength in the range of 19 to 26% at different burn-off percentages. This is attributed to the higher amount of oxide products formed during the activation process. At 600 °C, formation of the brittle Al_4C_3 phase in the different sintered composites containing activated and unactivated chars was identified by X-ray studies.

1. Introduction

As starting materials and processing costs are increasingly becoming a critical factor in materials development, previous and existing synthesis methods of composite materials are being re-evaluated by scientists for optimum applications at a reduced cost without impairing the product properties [1–4, 7, 19, 25]. The solid-state fabrication route in metal–matrix composites (MMC) synthesis is known to have several advantages over liquid metallurgy technique, and these can be exploited to fabricate cost-effective parts. One of these benefits include the use of lower temperatures resulting in less interaction between the matrix and reinforcement [1]. This yields composites with excellent interfacial properties because of greater latitude to control the matrix–reinforcement interaction. More composites such as a composite of SiC and Ti alloy, which otherwise, is impossible as SiC dissolves in the molten alloy [2], can also be produced. Elemental consolidation aids can also be homogeneously blended into the matrix particles which leads to improved compositional and microstructural control [3].

Although the production of specialty products requires the use of costly equipment, less time at processing the fabrication of sound final parts and the lower energy requirement go a long way to offset this factor [4]. Also, further attempts to control porosity and boundary precipitates have been based upon controlled compositional changes and careful application of the consolidation techniques. Smith and Froes [6] agree with other investigators [7] that particulate and discontinuous filament composites are easier and much less expensive to fabricate through powder metallurgy (PM) than continuous filament composites because good interfacial properties added to microstructural and compositional homogeneity are achievable. With these, PM methods alone can be used to develop particulate composite materials possessing the combination of properties required for any specific working conditions of the friction and autoparts assemblies. From the point of view of the various levels of porosities which they can produce, higher technology applications in military, aerospace, and special automobiles require parts (both heavy-duty, and of intricate nature) made from the high-cost hydrostatic

0022–2461

and isostatic compaction, hot dynamic compaction, or explosive compaction methods while the relatively low-cost methods of single compaction, double compaction, and mechanical deformation following hot pressing are used to produce parts for electromechanics, automobiles, and low-duty machinery [8].

Aluminium alloys are widely applied in transportation, construction and leisure fields because of their excellent combination of properties such as low density, high strength–weight ratio, good corrosion resistance, high thermal conductivity and good fabricability. Different cast Al alloys reinforced with particulates of mica [9–11], coconut shell char [12], graphite [13], SiC [14–16] and zircon sand [17, 18] have been studied and proposed for various automotive uses. Among the investigators, few [12, 14] have used the well-known cast-alloy, Al–Si. Besides, little work has been done on the introduction of these particulates to the alloy through conventional PM for cost-effective, similar applications [19, 20]. Recent advances on the Al–Si alloy PM particulate composites [21–23] employed only the use of relatively costly consolidation techniques to satisfy the various needs of aerospace, defence, and special automobile industries. Silicon imparts strength and low shrinkage to Al and this lends aluminium–silicon alloys to near net-shape processing, as is readily achieved in solid-state processes. Also, the use of an Al–Si alloy instead of pure Al as the matrix is also known to decrease the coefficient of thermal expansion of a composite with minimal reduction in thermal conductivity [24], which is a critical property in contact and electromechanical applications. These properties are also exploited for pistons, and the high hardness of the Si particle for wear resistance. The alloy becomes abrasion resistant at eutectic and hypereutectic (13–25 wt %) compositions with the additions of Ni, Cu, Mg, Mn, Co and Cr [25] because the presence of intermetallic phases cause good wear properties, high abrasion resistance and good heat resistance.

Coconut and palm-kernel shell chars are specially light and porous forms of carbon, currently being underutilized in Asia, India, and Africa. They are renewable and their resources in the world are expected to be more than 3 million tonnes. This work has therefore investigated the potential of these chars in hypereutectic Al–Si alloy through a low-cost, cold pressing powder technique for lightweight, contact applications. The process variables and the volume fractions were optimized and the applicable physical and mechanical properties determined.

2. Experimental procedure

2.1. Materials

In this synthesis, cold-pressed, double compaction PM processing was used. The major stages are elemental blending and mixing of the matrix powders and the reinforcements, pressing into green compacts, delubrication (or presintering), and sintering of the compacts. A flowsheet of these stages are schematically shown in Fig. 1. The matrix alloy powders, Al and Si, were supplied by the Aluminium Powder Co. Ltd (ALPOCO), West Midlands, UK, and by Goodfellow, Cambridge, UK respectively. They were analysed for elemental compositions using atomic absorption spectroscopy (AAS) and the results are as shown in Table I. The Al powder was produced by air-atomization, and Si, by comminution and milling.

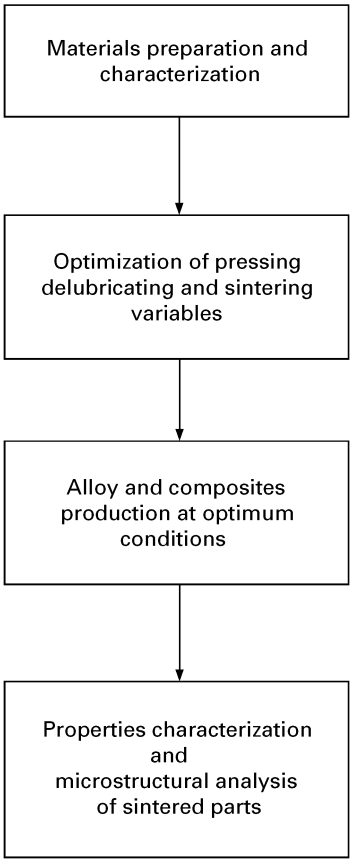

Figure 1 The processing method flowsheet.

TABLE I Composition (wt %) of Al and Si powders

Elements	Al powder	Si powder
Al	99.721	0.711
Si	0.028	98.001
Ca	–	0.276
Fe	0.150	0.314
Zn	< 0.010	–
Pb	< 0.010	–
Others	< 0.091	0.698

The organic precursors used in this work were coconut shells (aged < 1 year) and palm kernel shells (aged between 4 and 5 years), supplied from Uke Grains Ltd, Nigeria. Samples of the shells were milled and analysed for organic constituents. The results are shown in Table II. The shell fragments (approx: 4.5 kg) were primarily carbonized (charring) in a closed thick mild steel pot (without the use of a suitable gasket) for 3.5 h. A slit at the top end was provided for the insertion of the platinum–rhodium thermocouple used for reading the temperature. The maximum temperature of charring was 655 °C. Volatile gases, such as those of carbon and hydrogen, were recirculated in the pot and were condensed to solids. The carbonization process

was visually monitored and it was considered complete when the little escaping gases, with the lid in place, stopped. The pot was air-cooled and the chars removed. The chars were then analysed for elemental compositions using the CEC 240XA elemental analyser. The compositions are shown in Table III.

Size-reduction of the chars was carried out in the 0.25 HP NECO ball mill operated at 15–45 r.p.m. for about 1 h with alumina balls. A low speed range was found appropriate to avoid chipping of the alumina balls. A ball–charge ratio of 4 : 3 by volume was used. Further reduction was achieved in an alumina mortar with a silica mallet. Both the matrix powders and the chars were sized in an Endecott mechanical sieve shaker, and the particles of size less than 300 μm were used. Annealing of the powder samples for stress relief were carried out. Prior to mixing Al and Si powders, the blends were annealed under dry liquid nitrogen (dew point $-68\,^{\circ}C$, flow rate: 2.1 min^{-1}) at 350 °C in the case of Al, and at 190 °C for Si. The chars were also annealed under dry liquid nitrogen at 300 °C for 1 h. During the annealing process, the powder samples were placed in a silica glass plate having fine pores at the bottom to enable both the transfer of heat and passage of the gas.

The strength of oxidation of the chars during primary carbonization was determined through the energy dispersive X-ray analysis (EDXA), using the Link Systems-860 analyser. These results are shown in Fig. 2. Thermogravimetric analysis (TGA) of the matrix

TABLE II Composition (wt %) of coconut and palm-kernel shells

Constituents	Coconut shell powder	Palm-kernel shell powder
Moisture	12.00	6.72
Ash	0.62	1.10
Lignin	29.35	27.55
Solvent extracts	2.71	1.06
Pentosan	28.11	35.72
Cellulose	26.20	20.07
Anhydride	0.92	5.11
Others	0.09	2.68

TABLE III Composition (wt %) of coconut and palm-kernel shell chars

Elements	Coconut shell char	Palm-kernel shell char
C	77.15	71.66
H_2	2.88	2.62
N_2	0.24	0.59
S	< 0.1	< 0.1
P	0.018	0.047
Others	19.71	26.01

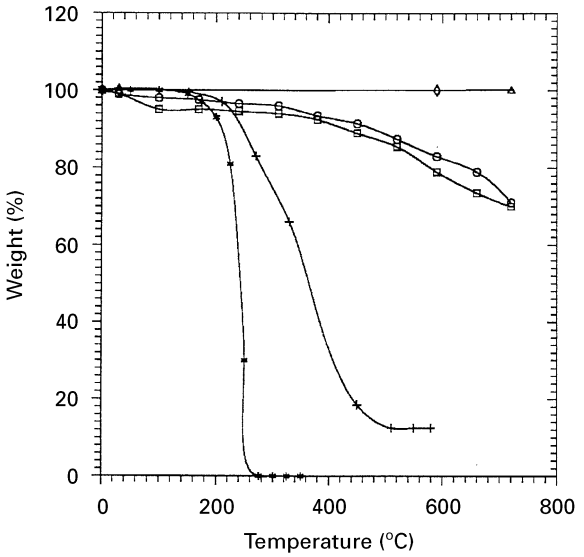

Figure 3 Thermogravimetric analysis of the matrix powders, char particles and lubricants under N_2 atmosphere. (◇) Al powder; (△) Si powder, (○) coconut shell char; (□) palm-kernel shell char; (+) AlSt powder; (*) stearic acid granules.

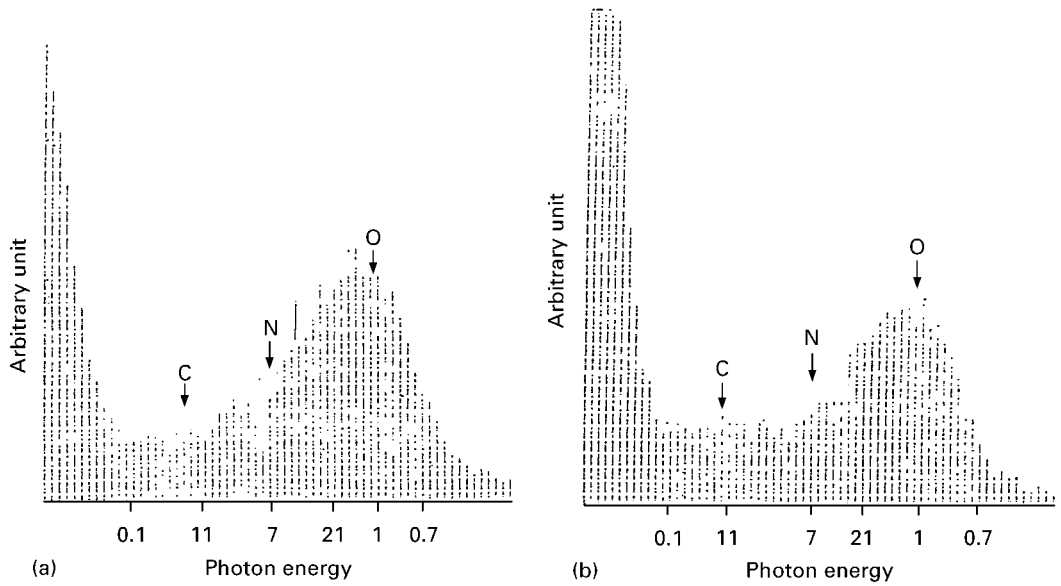

Figure 2 EDX analysis showing the amount of oxygen present after carbonization.

powders, Al and Si, as well as the lubricants used (stearic acid and aluminium stearate) and the chars were carried out under nitrogen atmosphere for their behaviour during the presintering stage. At the same ramp of 10 °C min^{-1}, the matrix powders were heated to 600 °C, the lubricants to 550 °C and the chars to 720 °C. These thermograms are shown in Fig. 3.

The densities and porosities of the powders were determined according to ASTM standards while the specific surface area, average particle size, and average pore size were measured by mercury porosimetry, using the Carlo Erba Strumentazione Porosimeter 2000. The pH of the chars were also measured using deionized water of pH 5.8, and this, together with the other characteristics, are given in Tables IV and V.

2.2. Cold pressing

Elemental blends of the matrix alloy powders, Al–13.5 wt % Si, were weighed and mixed. 1 wt % stearic acid (size 500 μm) was added as lubricant. Every 22.5 g of the mix was compacted to tensile bar specimens at pressure levels of 200, 250, 300, 350, 400, 450 MPa. At each pressure level, several green compacts were produced according to Metal Powder Industries Federation, MPIF 10–63 requirements. A double-action hardened steel mould and punch assembly was used. The pressing action utilized the Denison T42-B3 hydraulic press of 100 t capacity with the rate of application of pressure at 7 MPa s^{-1} and hold time of 3 s. Because of the high stripping pressure (200–300 MPa) experienced, die-wall lubrication with 0.5 wt % aluminium stearate was applied and this reduced the pressure to 45–180 MPa. The green densities of the compacts were determined and dimensions were measured.

2.3. Sintering

The green compacts were presintered (to remove lubricants) in a low dew-point (− 68 °C) liquid nitrogen atmosphere at 300 °C for 1 h using combined controlled sintering machine at ramp 10 °C min^{-1}. The samples were later furnace cooled to room temperature. Before any sintering operations of the study samples, it was necessary to determine the optimal sintering shedule for the alloy before any composites preparation. The various schedules tested have temperatures in the range 580 to 620 °C and hold times from 10 min to 2 h. High sintered density, high ultimate tensile strength (UTS) and little or lack of distortion (measured from dimensional changes) were used as determinants in choosing the optimal schedule. These results and the other measured characteristics are presented in Fig. 4a–f. Under nitrogen, the optimum schedule was: ramp 10 °C min^{-1}, hold temperature 600°C, dwell 15 min, cooling rate 17 °C min^{-1} to 180 °C, and then air cooling.

Under vacuum, the optimum schedule was the same as in nitrogen except the cooling rate which was 18 °C min^{-1}. The vacuum pump used consisted of an Edwards E2M5 rotary backing pump linked to an Edwards EXT 200 turbomolecular pump. The use of the turbomolecular unit meant that an almost totally hydrocarbon-free vacuum, variable from 1.33×10^{-1} to 1.33×10^{-4} Pa was available. Accordingly, the sintering in vacuum was achieved using the same (diffusion) pump at a tube pressure between 0.442 to 0.17 Pa and at backing pressure of 80 MPa. Because of deposition of lubricants on the tube during dewaxing in nitrogen, a different tube was used for sintering in vacuum in order to avoid sucking of the deposits into the diffusion pump thereby impairing its vacuum ability.

Based on the results, dewaxing in nitrogen at 300 °C for 1 h and sintering under vacuum according to the optimal schedule above were applied to the composites. The chemical composition of the sintered alloy is given in Table VI. The Al–13.5Si alloy was reinforced with the coconut shell char at five volume fractions: 0.7 vol %, 2.0 vol%, 4.0 vol %, 8.0 vol % and 12 vol %. At the same volume percentages, the alloy

TABLE IV The percentage burn-off, activation time, pH and composition (wt %) of activated coconut shell char

Sample	Burn-off (%)	Time (min)	pH	C	H_2	N_2	P	S
Unactivated	0.0	0	6.2	77.15	2.88	0.24	0.018	< 0.1
CA	21.7	105	6.9	88.59	0.44	0.22	–	< 0.1
CB	35.2	110	7.3	90.33	0.24	0.13	0.05	< 0.1
CC	40.5	160	7.3	90.33	0.20	0.07	0.02	< 0.1
CD	48.5	200	7.8	90.33	0.21	0.17	0.04	< 0.1

TABLE V The determined characteristics of the powders and chars

Characteristics	Coconut shell char	Palm-kernel shell char	Al	Si	Al–13.5Si
Apparent density (g cm^{-3})	0.6130	0.6236	1.08	1.05	1.09
Tap density (g cm^{-3})	0.8123	0.8179	1.31	1.40	1.37
Particle density (g cm^{-3})	0.8908	0.8432	2.62	1.85	–
pH	6.2	6.5	–	–	–
Total porosity (%)	50.64	67.80	36.05	66.15	48.68
Specific surface area (m^2 g^{-1})	1.61	3.16	1.77	0.35	4.21
Bulk density (g cm^{-3})	0.7	0.91	2.13	1.57	2.57
Average pore radius (nm)	17881	34535	3853	5942	37584

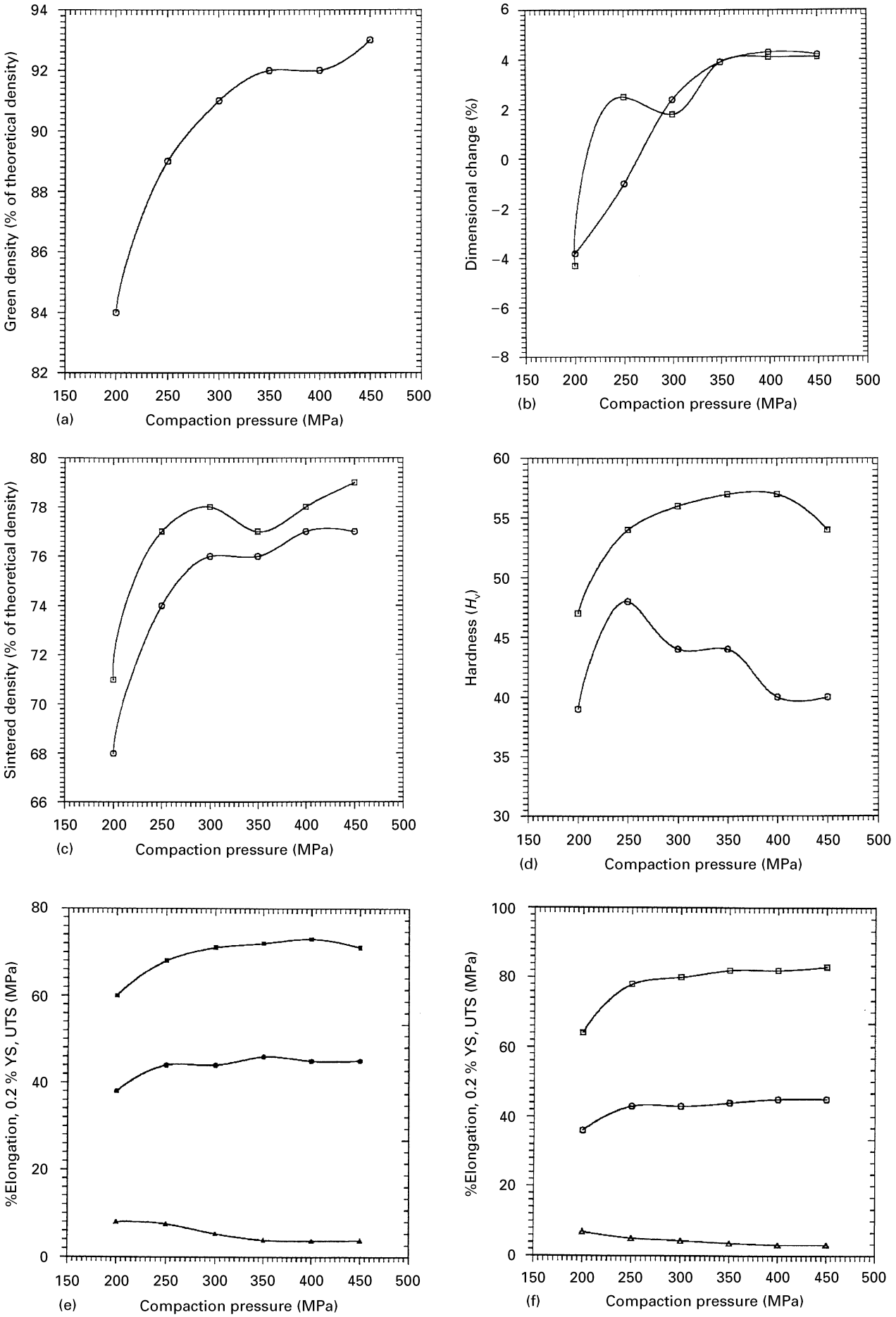

Figure 4 Effect of pressure on (a) green density; (b) dimensional change; (c) sintered density; (d) Vicker's hardness of sintered Al–13.5Si alloy parts; (□) vacuum-sintered; (○) nitrogen-sintered. Variation of the tensile properties of Al–13.5Si alloy sintered in (e) N_2 and (f) vacuum with compaction pressure; (□) UTS; (○) 0.2% YS; (△) % elongation.

TABLE VI Composition (wt %) of the matrix alloy

Element	Composition
Al	86.20
Si	13.52
Fe	0.13
Ca	0.002
Cu	0.003
Others	0.147

was also reinforced using palm-kernel shell char. Mg (2.5 wt %, size 100 μm) was added to the alloy as co-sinter. Tensile test-bars were compacted at 250 MPa, delubricated in nitrogen and sintered under vacuum. The tensile bars were supported on a wire gauze to achieve uniform heating of the bars, even diffusion of the nitrogen gas, and to allow free exit of the gasified lubricants.

2.4. Properties characterization

The heights of the sintered bars were remeasured along their gauge length. For each composite bar an average of five points was taken enabling the computation of the linear dimensional change. A sensitive electronic vernier calliper was used for this measurement. Because Mg forms amalgam with mercury, sintered density measurements were performed using light paraffin oil. This colourless liquid has a kinematic viscosity (at 37.8 °C) of $\leqslant 30 \times 10^{-5}\,m^2\,s^{-1}$. Percentage porosities were also determined.

The UTS, 0.2% yield strength (YS) and percentage elongation of the matrix alloy and the composites were tested using the 50 kN Instron Automated Materials Testing System, Type 4206, according to the ASTM designation: E8-81. Samples were prepared from the failed bars, and Vicker's hardness tests carried out using a load of 5 kg.

In order to investigate the effect of meso- and microporosity of the chars on the sintering behaviour of the composites, coconut shell char was activated under CO_2 at 915 °C after secondary carbonization in high-purity liquid nitrogen in a gravimetric tube furnace assembled from a Donaldson Vertical split tube furnace and a Cahn RH electrobalance. Samples were activated to burn off percentages between 21.7 and 48.5 and their pH values measured (see Table IV). They were analysed for elemental compositions, characterized by mercury porosimetry and used in filling the Al–13.5Si–2.5Mg alloy at 0.02 V_f (R1 to R4). Similar properties that were determined in the alloys were also determined in the composites. The composites containing 0.02 V_f (volume fraction) coconut shell char (activated and unactivated) characterized for phase using the Sietronics X-ray diffractometer.

3. Results and discussion

3.1. Materials

It was observed that the fragments near the walls of the pot charred more than those near the centre as heating was from one direction. The relatively high amounts of moisture and solvent extracts as well as the low ash content (Table II) could be attributed to the nature and age of the shell species. X-ray studies (Fig. 2) confirm oxygen pick-up which affected the percentage of elemental carbon present as shown in Table III. As could be seen from Table IV, the coconut shell char improved its carbon yield on activation by an average of about 14.8% which is attributed to the removal of moisture and volatiles as well as burning away of sacreligious and inorganic substances. The thermograms in Fig. 3 reveal that 100% of the stearic acid, $CH_3(CH_2)_{16}COOH$, at 280 °C and 87% of AlSt, $(C_{17}H_{35}\cdot COO)_3Al$, at 510 °C, were removed under nitrogen. This means that all the lubricants were driven off during the sintering and not during the presintering stage. At the delubrication temperature (300 °C) in nitrogen, only negligible weight loss of the chars (and none in the case of the matrix powders) was observed.

As shown in Table V, the apparent densities of all the powders are less than their respective tap densities. This agrees with the conclusion by Hausner [26] from his work on metal and ceramic oxide powders. The high particle density of Al powders indicate a very low population of open and closed pores. The pH values of the chars indicate that charring reduced their acidity, suggesting that large quantities of volatiles, carboxylic group and moisture were eliminated. This is confirmed by the increment in pH of the activated coconut shell chars to an average of 7.3 as given in Table IV. Spherical, globular shaped aluminium particles are typical of air-atomized powders and the angular structure of silicon particles is also typical of milled ductile particles. The char particles are observed to be irregular shaped which are typical of milled hard and brittle powders. A high surface area of the alloy premix in comparison to those of Al and Si powders, shown in Table V, was observed. Increased surface areas have been reported of powder premix with spherical/angular particles and having large and small sizes [27].

3.2. Physical properties

Fig. 4a shows that the green density of the compacts increases at a decreasing rate with pressure, and it is attributed to initial rearrangement of particles and then, to plastic deformation of powders and the abrasion resistance of surface films present. At 250 MPa, a green density 89% of the theoretical value was achieved by our alloy compacts. At pressure levels above 350 MPa, green density of about 91% theoretical density, was also achieved. In his work on Al powders, Kehl [28] achieved a green density of about 90% at pressures above 250 MPa. Dudas *et al.* have earlier [29] reported that a density of 90–94% theoretical density ensures satisfactory strength in Al powder parts. The differences in the crystal structure of the matrix powders (Al is f.c.c. and Si has diamond structure) as well as that of the lubrication powders and method of lubrication are suspected to account for the apparent variations. On the other hand, sintered density increased marginally with compaction pressure, as shown in Fig. 4c. However, alloys compacted at

pressures less than 250 MPa experienced shrinkage while those at higher pressures experienced swelling after sintering under vacuum (see Fig. 4b). A similar pattern of behaviour was observed when sintered in nitrogen. The gases that were entrapped, as well as the lubricants that were compressed because of high pressure, may have given rise to swelling while particle reorientation effects are suspected to result in shrinkage.

As can be deduced from Fig. 4d–f, increase in compaction pressure resulted in marginal increase in indentation hardness, UTS and 0.2% YS of the unreinforced alloys. This suggests that sintered density has a direct relationship with mechanical properties which is in agreement with the report by Mulhearn and Samuels [30]. The measured YS (36–45 MPa) of the Al–13.5Si alloys sintered in either vacuum or N_2 were not high. Aluminium is known to possess lower yield strength because of their large number of slip planes. The size of stearic acid used, non-uniform compaction and presence of pores in the alloy compacts may have affected the mechanical property values attained. Pores and shrinkage cavities are regions of discontinuity for load transfers. The measured difference in dimensional changes between the coconut-char reinforced composites (C-series) and the palm kernel char reinforced composites (P-series) is marginal. As shown in Fig. 5b, shrinkage decreases as more chars are added. At 0.12 V_f, the composites exhibited poor handling strength. At about this value, the sintering influence of 2.5 wt % Mg by particle surface modifications was inadequate for the increased total surface area of the char particles. Wetting and subsequent bonding became minimal and highly localized. The sintered densities (Fig. 5a) of the composites showed direct relationship with dimensional changes suggesting that similar factors affect them. According to Kehl [28], the factors affecting densification during sintering include solid-state material transport through diffusion processes, evaporation and condensation of gases, wetting of various phases as well as particle shape and particle size distribution. Also, apart from the role of Mg in raising the surface energies of the particles reactions, the high surface area (due primarily to finer particle size) of the chars and of the alloy may have been largely responsible for the density achieved. This is corroborated by the measured marginal increase in the sintered density of the composite filled with 0.02 V_f following the addition of more than 1 wt % Mg to our matrix alloy (from 77 to 78% of theoretical density).

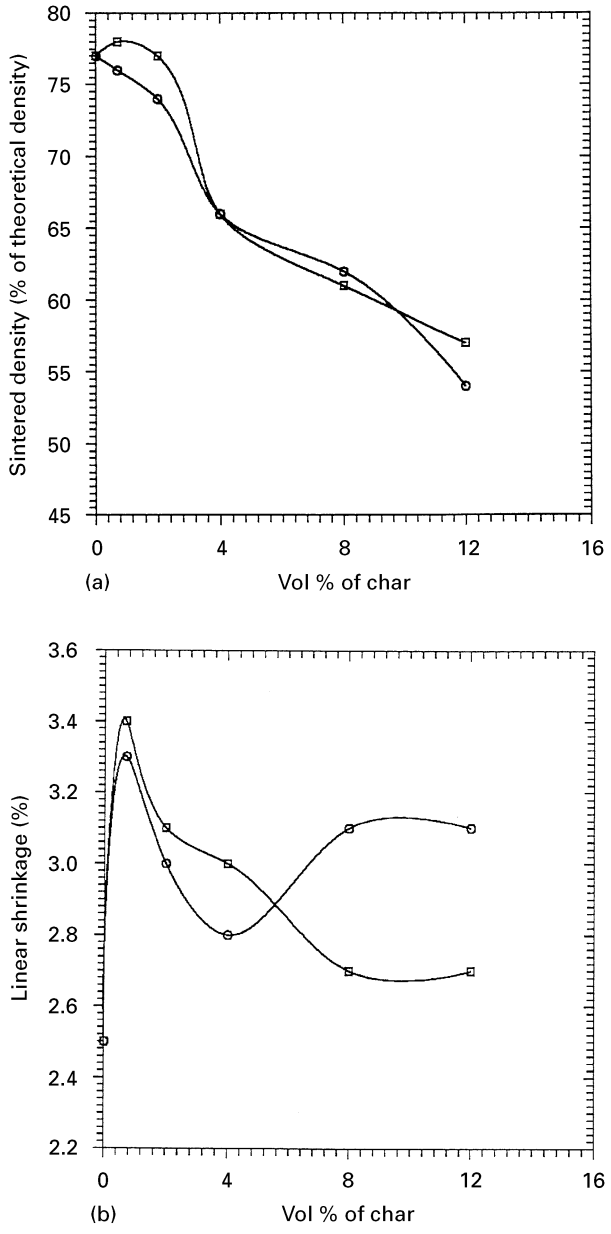

Figure 5 Effect of (a) chars on sintered density and (b) linear shrinkage of sintered Al–13.5Si–2.5Mg alloy composites. (□) Coconut shell char; (○) palm-kernel shell char.

3.3. Mechanical properties

The UTS, YS and percentage elongation of the alloy decreased with progressive additions of the chars as shown in Fig. 6a–b. The tensile strength, modulus, hardness, and thermal expansion of coconut shell chars [34] are much lower than those of our matrix alloy. There is only a marginal difference in these values between the C-series and P-series composites. This difference is suspected to have arisen from the differing particle characteristics and the nature of porosities in the two types of composites. The pore distribution in the P-series may have been relatively non-uniform. Reduction in mechanical properties of Al-based alloys because of additions of coconut shell char and granular graphite have been reported by previous investigators [12, 13]. Factors suspected to contribute to the reduction in these properties are attributed to: (1) lower strength of the dispersed char particles; (2) the porosity of the parts (the highest density achieved being only 78% of theoretical); and (3) the decrease in the specific strength (strength/density) of the composites caused by the increasing weakness of the interfacial bonds with additions of char. The wettability of the particle surfaces by magnesium is thought to reduce with increasing amounts of the char particles. The measured hardness (in Fig. 6c) are not in their high values (25–57 H_v). Jha and coworkers have earlier reported low hardness values for graphite-reinforced Al alloy composites sintered in

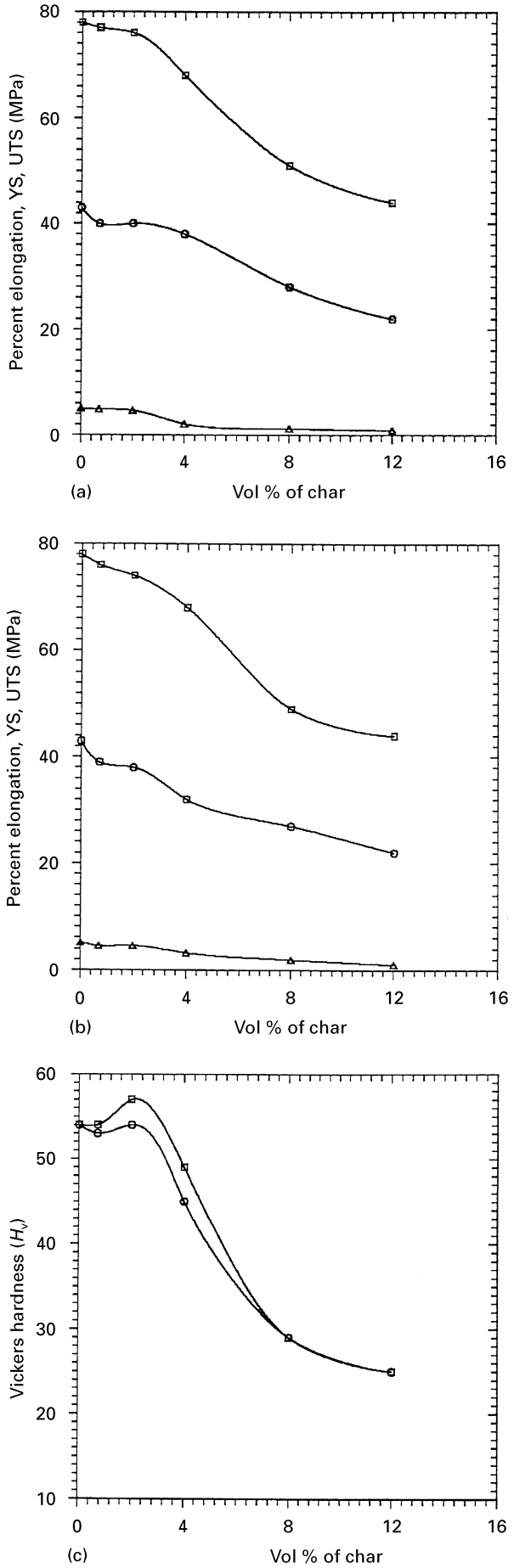

Figure 6 Effect of (a) coconut shell char and (b) palm-kernel shell char on tensile properties of Al–13.5Si–2.5Mg alloy composites. (□) UTS; (○) YS; (△) % elongation. (c) Effect of char particles on hardness of sintered Al–13.5Si–2.5Mg alloy composites. (□) Coconut shell char, (○) palm-kernel shell char.

a low dew-point ($-68\,^{\circ}C$) N_2 [19]. The peaking up of Vicker's hardness at 0.02 V_f of the reinforcement may be representative of an optimum volume fraction arising from good bonding and the nature of reduced porosity in our composite. At this V_f, our earlier work [5] has reported that both the coefficient of friction and the adhesive wear rate (under dry conditions) were significantly reduced by 51 and 77%, respectively, and that its coefficient of linear thermal expansion at 25–100 °C was found to reduce from 21×10^{-6} to $11.7 \times 10^{-6}\,^{\circ}C$.

3.4. Effect of activated coconut shell char

The characteristics and properties of the composites reinforced with activated coconut shell chars are given in Table VII(a–b). The sintered densities of the composites (R1 to R4) decrease with burn-off, from 75% at 21.5% burn-off to 70% at 48.5% burn-off in spite of high reactivity of chars. Poor wetting of the chars resulting from insufficient amount of Mg which did not promote significant reducing reactions with oxide products are considered responsible. There was no significant difference in the wear rates and coefficients of friction of the composites both from one another and from the composite containing unactivated char (Table VII). The procedures used for the dry adhesive wear and thermal expansion tests are described

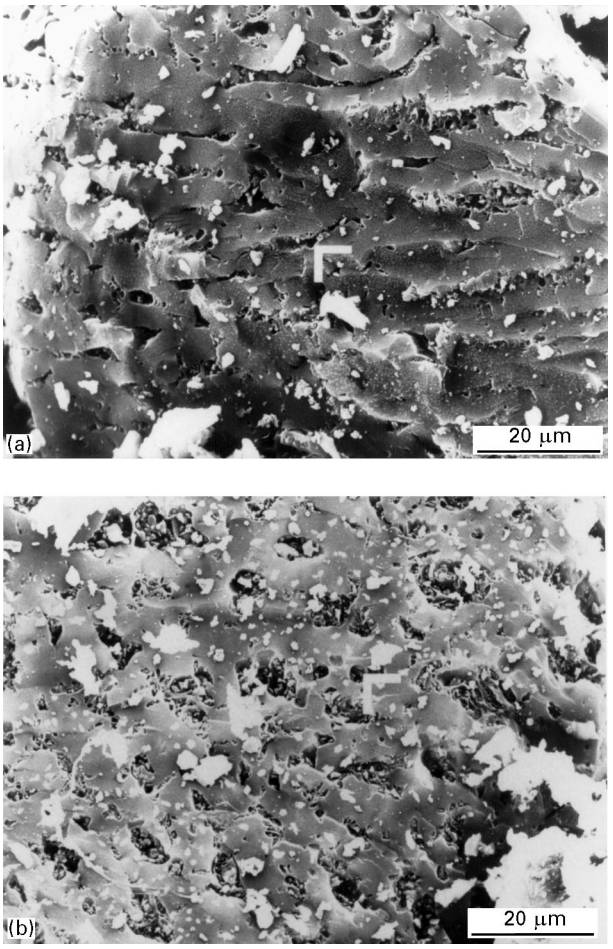

Figure 7 SEM of activated coconut shell char at (a) 21.7% (CA) and (b) 48.5% burn-off, revealing many pores and ash deposits (white colour).

TABLE VII (a) Characteristics and (b) tensile properties of Al–13.5Si–2.5Mg alloy reinforced with 0.02 V_f unactivated (C2) and activated coconut shell char at burn-offs of 21.7% (R1), 35.2% (R2), 40.5% (R3) and 48.5% (R4)

Composites	Sintered density (% relative)	Porosity (%)	Linear shrinkage (%)	Wear-rate ($g\,cm^{-1} \times 10^{-7}$)	Coefficient of friction	Coefficient of linear expansion ($K^{-1} \times 10^{-6}$)
C2	77	23	3.1	1.7	0.61	11.7
R1	75	25	1.1	1.8	1.8	19.24
R2	73	27	0.9	1.8	1.8	20.76
R3	73	27	0.4	1.5	1.5	16.91
R4	70	30	0.4	1.7	0.5	15.50

Composite	UTS (MPa)	0.2% YS (MPa)	Elongation (%)	Hardness (H_v)
C2	76	40	4.7	57
R1	63	31	1.4	56
R2	62	32	2.0	55
R3	58	30	1.0	50
R4	58	29	1.0	50

elsewhere [5]. There was a progressive decrease in thermal expansion with activation time. At higher burn-off percentages, 40.5 and 48.5%, the coefficient of linear thermal expansion of the composites (R3 and R4, respectively) containing 0.02 V_f composition decreased by an average of 16%. The created pores served as sinks to thermal transport of atoms and materials.

The measured mechanical properties shown in Table VIIb do not show any significant difference from the C2 composites. Scanning electron microscope (SEM) micrographs of CA and CD (activated to 21.7 and 48.5% burn-off) are shown in Fig. 7 revealing the micropores and mesopores (arrowed) which are created (on activation) due to the oxidation of carbon atoms in the active site. Although mercury porosimetry is also applicable and was used in this work, it is commonly applied in determining mesopores (size, between 3 and 200 nm) and macropores (size $>$ 200 nm). Electron probe microanalysis (EPMA) on CA and CD identified the white deposits in the micrographs as oxides of Cu and K which are suspected to have hindered good sintering. The identification of these oxides is explained from the visibly observed little amount of ash after the activation cycles of the chars. Ash is known to consist of alkali oxides (such as K and Cu), alkaline earthoxides and silica [12]. It is not possible for Mg at the operating temperature, given its free energy of formation of oxides, to reduce these oxides. Also, the low amount of Mg used is suspected to have been reduced at the operating pressure of our vacuum.

3.5. Fracture and phase formation

In the X-ray diffraction patterns of C2 and R4 presented in Fig. 8, aluminium carbide crystal peaks are observed. They correspond to the third strongest line of the crystalline interphase compound. An earlier work [31] had, however, reported that unless the mixture of aluminium and carbon is subjected to explosive shock under pressure, or wetted with cryolite, carbide formation below 1000 K is very sluggish during carburization of aluminium. It was also observed, by this method of analysis, that activation of the chars did not affect the strength of the peak of this brittle phase which confirms the possibility that more reactions were not promoted when more pores were created. According to Mondolfo [32], amorphous and/or crystalline Al_4C_3 can be formed in Al–C systems according to the reaction $3C + 4Al \Rightarrow Al_4C_3$. At our sintering temperature ($600 \pm 2\,^{\circ}C$), it is possible that the vacuum attained as well as the gasified lubricants have affected the activity of aluminium, which also explains the negligible effect of the activated chars on the amount of carbide formed. The thermodynamics of this reaction are being investigated.

A typical fractograph of C2 composite after tensile test is shown in Fig. 9. There are no voids around the particles. There appear to be irregularly shaped voids in the matrix with formations of dimples, indicating that the matrix appears to have failed by ductile fracture. This agrees with the observation by Murali *et al.* [12]. In the zones where char partiles (arrowed) are exposed, brittle fracture is seen and the fracture path seems to have traversed across the interface.

Rigid fillers such as carbon, zircon and alumina in the soft matrix of Al–Si alloys cannot deform sufficiently and may easily become debonded, losing their ability to bear the load [17]. Similar dispersion of rigid particulate fillers such as glass beads, alumina and thermoplastic powder in the soft epoxy resin matrices have been reported to induce tensile stress concentrations, altering the fracture behaviour and therby enhancing shear yielding [33]. Therefore, the use of the Nicholas relation could be made to determine the predominant mode of fracture in our composites. According to the Nicholas relation [34].

$$\alpha = \alpha_m(1 - a\delta^n)$$

where α = strength value of the composite; α_m = strength value of the matrix; δ = volume fraction of

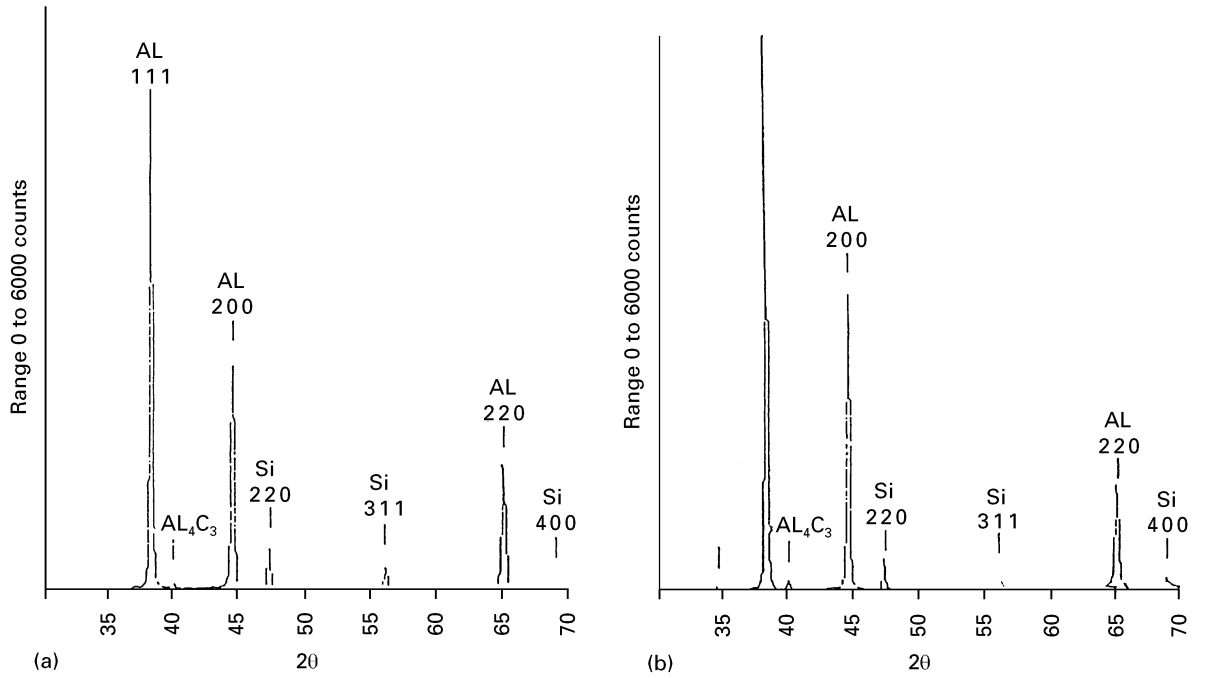

Figure 8 X-ray diffraction pattern of sintered Al–13.5Si–2.5Mg alloy reinforced with 0.02 V_f of (a) unactivated coconut shell char and (b) 48.5% burn-off activated coconut shell char, revealing aluminium carbide, Al_4C_3 phase formation.

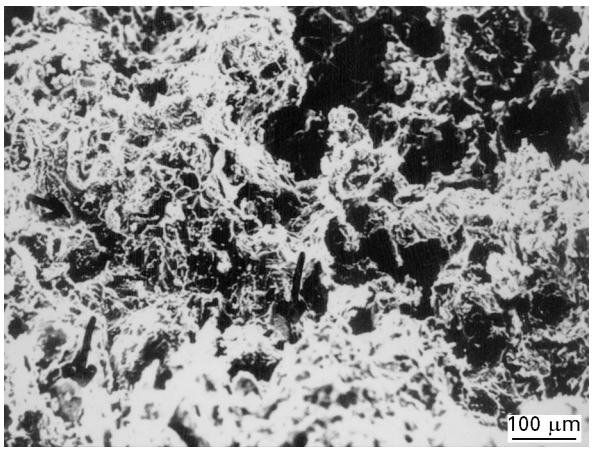

Figure 9 Typical SEM of sintered char-reinforced Al–13.5Si–2.5Mg alloy composite indicating both ductile and brittle failures.

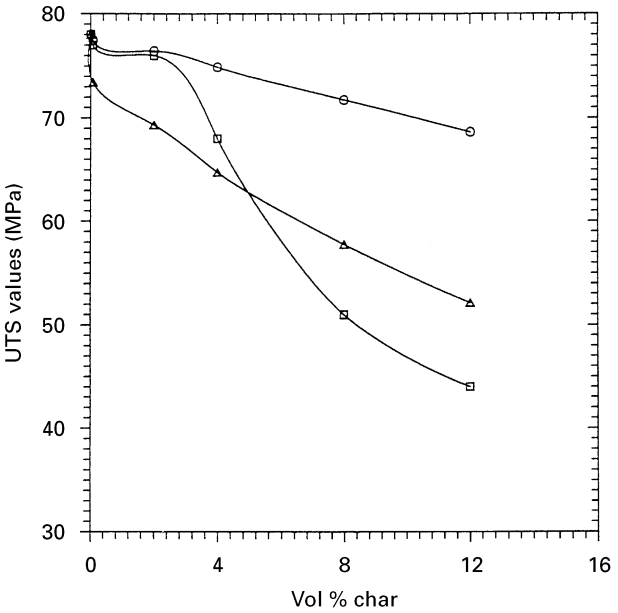

Figure 10 Comparison of measured and theoretically computed UTS values of char-reinforced Al–13.5Si–2.5Mg alloy composites according to the Nicholas relation, indicating a predominantly brittle failure at high volume fractions of char. (○) upper boundary; (□) measured; (△) lower boundary.

the second phase particles for spherical particles in a polymer matrix; a and n are constants; and $a = 1$, $n = 1$, upper bound, when fracture path is perfectly random; $a = 1.21$, $n = 0.61$, lower bound, when fracture path deviates through the equiaxial plane of spheres, the mode of fracture can be related to the strength analysis of the composites. Fig. 10 compares the theoretically computed strength values with the measured values. It can be seen that the measured values are nearly in close agreement with the values generated using the lower bound constants of his equation. The observation from the fractograph corresponds with this analysis. This failure at the interface is explained from the nature of the thick reaction zone formed at the interface. Continued reaction to form a new compound at the interface is known to be generally more degrading to the properties of a composite than simple solution. In such a condition the strength of the reaction zone will be lower than that of the reinforcement so that when the compound is brittle, its strain-to-fracture will be lower than that of the reinforcement particle. The cracks formed in the reaction layer at this strain determine the mechanical behaviour of the composite. According to Lyle [35], because the bonding is accomplish without benefit of metalworking, then voids, oxides, and solute-rich phases are concentrated at the interfaces providing fracture path. An earlier study [5] on the interface between the chars and the matrix revealed formations of silicides of Mg and Al. Optimum interfacial product for useful properties was observed at 0.02 V_f when

2.5 wt % Mg was added. It also reported that the least interparticle distance was found to be 200 μm [5].

4. Conclusions

The use of the conventional, low-cost, double compaction PM route in the fabrication of Al–Si alloy particulate composites is still viable and fundamental to achieving cost-effective, lightweight automotive composite parts. Reinforcing the hypereutectic Al–13.5Si–2.5Mg alloy with coconut shell char at 0.02 V_f and sintering the composite at 600 °C in vacuum for 15 mins, following a net shape compaction at 250 MPa, only marginally reduced the UTS of the alloy from 78 MPa to 76 MPa, 0.2% YS from 43 to 40 MPa and percentage elongation from 5.1 to 4.7. The hardness of the alloy increased by only 6%. The use of palm-kernel shell char as the filler phase were found to yield only identical results. At 0.02 V_f of coconut shell char, the mechanical properties, sintered density and dimensional changes were found to be optimum, and suitable for lightweight anti-friction electromechanical applications. Further work is, however, necessary to evaluate their relevant electrical and thermal properties. Attempts to reinforce the alloy with coconut shell chars activated in CO_2 resulted in reduction in linear shrinkage and mechanical properties of the unreinforced alloy. This is attributed to insufficient reduction of the new oxide products by the available sintering aid, Mg. At about 600 °C, formations of the brittle Al_4C_3 phase in the different sintered composites containing activated and unactivated chars were identified by X-ray analysis. This phase formation is caused by the reaction between the matrix and the carbon produced during the reaction sintering stage. The concentration of Al_4C_3 formed was found to be independent of the porosity of the chars.

Acknowledgements

We are pleased to acknowledge the financial support of this research by National Science Foundation, grant No., DMR-9314016. We also thank Professor Brian Ralph and the staff of the Department of Materials Technology, Brunel University, Uxbridge, UK for their assistance in carrying out some part of this research work.

References

1. J. S. CROMPTON and R. W. HERTZBERG, *Mater. Sci.* **21** (1986) 3445.
2. Y. ABE, M. NAKATANI, K. YAMATSUTA, and S. HORIKIRI, in Procedings of a Conference on Developments in the Science and Technology of Composite Materials, Bordeaux, 1985, edited by A. R. Bunsel, P. Lamicq and A. Massiah (EACM, Bordeaux, 1985) p. 604.
3. J. U. EJIOFOR, B. A. OKORIE and R. G. REDDY, *J. Mater. Engng Perf.* **6** (1997) 326.
4. P. J. JANIS, *Met. Powder Rep.* **44** (1989) 369.
5. J. U. EJIOFOR and R. G. REDDY, in Proceedings of Conference on Automotive Alloys, Orlando, FL, February 1997, edited by S. K. Das (TMS, Warrendale, 1997) p. 95.
6. P. R. SMITH and F. H. FROES, J. Metals **March** (1984) 19.
7. A. NIKLOS, L. FROYEN, L. DELAEY and L. BUEKENHOUT, *Mater. Sci. Engng A.* **135** (1991) 225.
8. V. S. ARUMACHALAM and B. V. ROMAN, in "Powder metallurgy – recent advances" (Aspect Publishers, London 1990) p. 124.
9. D. NATH and P. K. ROHATGI, *J. Mater. Sci.* **16** (1981) 1579.
10. A. K. GUPTA, T. K. DAN, and P. K. ROHATGI, *J. Mater. Sci. Lett.* **6** (1987) 35.
11. D. NATH, R. ASTHANA and P. K. ROHATGI, *ibid.* **22** (1987) 170.
12. T. P. MURALI, M. K. SURAPPA and P. K. ROHATGI, *Met. Trans.* **13B** (1982) 485.
13. U. T. S. PILLAI, PhD Thesis, IIT, Dehli, 1986.
14. J. YANG and D. D. L. CHUNG, *J. Mater. Sci.* **24** (1989) 3605.
15. D. J. LLOYD, in Proceedings of Conference on High Performance Composites for the 1990s, edited by S. K. Das (TMS, Warendale, PA, 1990) p. 33.
16. *Idem., Comp. Sci. Technol.* **35** (1989) 159.
17. U. T. S. PILLAI and R. K. PANDEY, *Comp. Sci. Technol.* **40** (1991) 333.
18. A. M. BANERJI, M. K. SURAPPA and P. K. ROHATGI, *Metall. Trans.* **14B** (1983) 273.
19. A. K. JHA, S. V. PRASAD and G. S. UPADYAYA, *Powder Metall.* **32** (1989) 309.
20. T. T. LONG, T. NISHIMURA, T. AISAKA and M. MORITA, *Mater. Trans.* **32** (1991) 181.
21. DWA Composite Specialties, Inc., Report, British Petroleum Metall. Composites, Farnborough, March (1990) p. 1.
22. H. J. RACK, in Proceedings on Processing and Properties of Powder Metallurgy Composites, edited by P. Kumar, K. Vedular and A. Ritter (TMS, Warrendale, PA, 1988) p. 155.
23. S. KRISHNAMURTY, Y. W. KIM, G. DAS and F. H. FROES, in Proceedings on Metal–Ceramic Matrix Composites: Processing, Modelling, and Mechanical Behavior, edited by R. B. Bhagat, A. H. Claver, P. Kumar and A. M. Ritter (TMS/Materials Society, Warrendale, PA, 1990) p. 145.
24. M. K. PREMKUMAR, W. H. HUNT, Jr and R. R. SAWTELL, *J. Metals* **July** (1992) 24.
25. S. AHMED, V. GOPINATHAN, and P. RAMAKRISHAN, in Proceedings of Conference on Cast Reinforced Metal Composites, Chicago, IL, (ASM, Metals Park, OH, 1988) p. 149.
26. H. A. HAUSNER, in "Handbook of metal powders", edited by A. R. Poster (Renhold Publishing Corporation, New York, 1966) p. 1.
27. J. LIBSCH, R. VOLTERA and J. WULFF, *Powder Metall*, **10** (1976) 379.
28. W. KEHL, M. BUGAJSKA and H. F. FISCHMEISTER, *ibid.* **26** (1983) 221.
29. J. H. DUDAS and C. B. THOMPSON, in "Modern development in powder metallurgy", vol. 5 (Plenum Press, New York, 1971) p. 19.
30. T. O. MULHEARN and L. E. SAMUELS, *Wear* **5** (1982) 478.
31. M. K. AGHAJANIAN, M. A. ROCAZELLA, J. T. BURKE and S. D. KECK, *J. Mater. Sci.* **26** (1991) 447.
32. L. F. MONDOLFO, "Aluminium alloys, structures and properties" (Butterworth Publishers, London, 1976) p. 237.
33. A. J. KINLOCH, D. A. MAXWELL and R. J. YOUNG, *J. Mater. Sci.* **4** (1985) 1276.
34. L. NICHOLAS, *Polym Engng Sci.* **15** (1975) 137.
35. J. P. LYLE, Jr, *Prog. Powd. Metall.* **28** (1972) 93.

Received 21 October 1996
and accepted 12 September 1997